

# Northumbria Research Link

Citation: Feng, Huijuan, Lv, Weilin, Ma, Jiayao, Chang, Wenwu, Chen, Yan and Wang, Jianshan (2020) Helical structures with switchable and hierarchical chirality. Applied Physics Letters, 116 (19). p. 194102. ISSN 0003-6951

Published by: American Institute of Physics

URL: <https://doi.org/10.1063/5.0005336> <<https://doi.org/10.1063/5.0005336>>

This version was downloaded from Northumbria Research Link:  
<http://nrl.northumbria.ac.uk/id/eprint/43927/>


Northumbria University has developed Northumbria Research Link (NRL) to enable users to access the University's research output. Copyright © and moral rights for items on NRL are retained by the individual author(s) and/or other copyright owners. Single copies of full items can be reproduced, displayed or performed, and given to third parties in any format or medium for personal research or study, educational, or not-for-profit purposes without prior permission or charge, provided the authors, title and full bibliographic details are given, as well as a hyperlink and/or URL to the original metadata page. The content must not be changed in any way. Full items must not be sold commercially in any format or medium without formal permission of the copyright holder. The full policy is available online: <http://nrl.northumbria.ac.uk/policies.html>

This document may differ from the final, published version of the research and has been made available online in accordance with publisher policies. To read and/or cite from the published version of the research, please visit the publisher's website (a subscription may be required.)

# Helical structures with switchable and hierarchical chirality

Cite as: Appl. Phys. Lett. **116**, 194102 (2020); <https://doi.org/10.1063/5.0005336>

Submitted: 20 February 2020 . Accepted: 30 April 2020 . Published Online: 14 May 2020

Huijuan Feng , Weilin Lv, Jiayao Ma, Wenwu Chang, Yan Chen , and Jianshan Wang



View Online



Export Citation



CrossMark

## ARTICLES YOU MAY BE INTERESTED IN

[Ghost imaging second harmonic generation microscopy](#)

Applied Physics Letters **116**, 191101 (2020); <https://doi.org/10.1063/1.5144690>

[Developing silicon carbide for quantum spintronics](#)

Applied Physics Letters **116**, 190501 (2020); <https://doi.org/10.1063/5.0004454>

[Monolithically fabricated tunable long-wave infrared detectors based on dynamic graphene metasurfaces](#)

Applied Physics Letters **116**, 191102 (2020); <https://doi.org/10.1063/5.0007780>

Lock-in Amplifiers  
up to 600 MHz



Watch



# Helical structures with switchable and hierarchical chirality

Cite as: Appl. Phys. Lett. **116**, 194102 (2020); doi: [10.1063/5.0005336](https://doi.org/10.1063/5.0005336)

Submitted: 20 February 2020 · Accepted: 30 April 2020 ·

Published Online: 14 May 2020



View Online



Export Citation



CrossMark

Huijuan Feng,<sup>1,2,3</sup>  Weilin Lv,<sup>1,2</sup> Jiayao Ma,<sup>1,2</sup> Wenwu Chang,<sup>4</sup> Yan Chen,<sup>1,2,a)</sup>  and Jianshan Wang<sup>2,5</sup>

## AFFILIATIONS

<sup>1</sup>Key Laboratory of Mechanism Theory and Equipment Design of Ministry of Education, Tianjin University, Tianjin 300072, China

<sup>2</sup>School of Mechanical Engineering, Tianjin University, Tianjin 300072, China

<sup>3</sup>Reconfigurable Robotics Lab, École Polytechnique Fédérale de Lausanne (EPFL), 1015 Lausanne, Switzerland

<sup>4</sup>Shanghai Putuo Modern Educational Technology Center, Shanghai 200062, China

<sup>5</sup>Tianjin Key Laboratory of Modern Engineering Mechanics, Department of Mechanics, Tianjin University, Tianjin 300072, China

<sup>a)</sup>Author to whom correspondence should be addressed: [yan\\_chen@tju.edu.cn](mailto:yan_chen@tju.edu.cn)

## ABSTRACT

Chirality is present as a trend of research in biological and chemical communities for it has a significant effect on physiological properties and pharmacological effects. Further, manipulating specific morphological chirality recently has emerged as a promising approach to design metamaterials with tailored mechanical, optical, or electromagnetic properties. However, the realization of many properties found in nature, such as switchable and hierarchical chirality, which allows electromagnetic control of the polarization of light and enhancement of mechanical properties, in man-made structures has remained a challenge. Here, we present helical structures with switchable and hierarchical chirality inspired by origami techniques. We propose eggbox-based chiral units for constructing homogeneous and heterogeneous chiral structures and demonstrate a theoretical approach for tuning the chirality of these structures by modulating their geometrical parameters and for achieving chirality switching through mechanism bifurcation. Finally, by introducing a helical tessellation between the chiral units, we design hierarchical structures with chirality transferring from construction elements to the morphological level and discover a helix with two zero-height configurations during the unwinding process. We anticipate that our design and analysis approach could facilitate the development of man-made metamaterials with chiral features, which may serve in engineering applications, including switchable electromagnetic metamaterials, morphing structures, and bionic robots.

© 2020 Author(s). All article content, except where otherwise noted, is licensed under a Creative Commons Attribution (CC BY) license (<http://creativecommons.org/licenses/by/4.0/>). <https://doi.org/10.1063/5.0005336>

Chirality refers to the asymmetric configurational property of an object, indicating that the object is unable to be superposed onto its mirror image.<sup>1</sup> Chirality is typically realized morphologically at the macro-scale by a helix—a structure that exists widely in both biological and artificial materials.<sup>2</sup> Chirality endows materials with unusual mechanical, optical, and electromagnetic properties and functions,<sup>3–6</sup> such as superior elasticity,<sup>3,4</sup> negative refraction,<sup>5</sup> and asymmetric electromagnetic wave transmission.<sup>6</sup> Recently, manipulation of chirality has provided an effective way to tailor these physical properties of materials.<sup>7,8</sup> Furthermore, some researchers designed metamaterials with tunable chirality based on deformation of existing origami patterns, such as Muira-ori<sup>9</sup> and Kresling.<sup>10</sup> Because of their unusual properties, chiral materials have widespread applications, such as in beam splitters,<sup>11</sup> circular polarization detectors,<sup>12</sup> and nanoelectromechanical systems.<sup>13</sup>

Chiral structures have either right-handed (RH) or left-handed (LH) chirality. Switching between these configurations has been observed in many biological<sup>14,15</sup> or chemical<sup>16,17</sup> processes. Besides achieving

particular biological functions,<sup>18</sup> chirality switching would be beneficial for engineering materials since it allows electromagnetic control of the light polarization and enhancement of mechanical properties. For example, materials with different handedness have different transmission effects on circularly polarized electromagnetic waves.<sup>6,11,19–21</sup> Such a property could be useful for light-splitting devices and detectors.<sup>11,12</sup>

The existing chirality switching is a molecular structural change induced by external stimuli in various natural<sup>15,16</sup> or artificial<sup>14,17</sup> materials. However, this would entail great complexity in manufacturing and difficulty in controlling structural reconfiguration. A photoinduced handedness switching without introducing any structural change was achieved in an artificial chiral metamolecule, but it still requires a photoactive medium.<sup>22</sup>

Chirality can also exist at multiple scales in the same structure, which is referred to as hierarchical chirality. The hierarchy of chirality is beneficial for the synthesis and properties of materials, for example, for symmetry control in morphogenesis and enhancing mechanical

properties.<sup>23,24</sup> In some biological structures, such as the bacterial flagella, chirality can be transferred from the nanoscale molecular level to the macroscale morphological level.<sup>4,25–27</sup> Hierarchical chirality also exists at the same scale, for instance, in carbon nanotube ropes,<sup>23</sup> synthetic polymeric nanobristles,<sup>24</sup> and insulin amyloid fibrils.<sup>28</sup> These structures are all coiled bundles assembled by uncluttered elements. Both switchable and hierarchical chiralities provide an effective way to tailor mechanical, optical, or electromagnetic properties of a material. However, they were studied separately and have never been achieved before with a single design.

In this Letter, we propose helical structures with tunable chirality based on an origami-inspired chiral unit. We demonstrate theoretically and validate experimentally the variation in chirality by adjusting geometric design parameters. We realize chirality switching in a single helix via mechanism bifurcation without any external stimulus and propose a hierarchically chiral structure with two zero-height configurations.

To achieve the helical morphology of chiral structures, we constructed a twisted origami unit. The basic origami pattern used here is an eggbox, a non-developable four-crease pattern. Two identical eggboxes are placed symmetrically to construct a chiral unit [Fig. 1(a) (Multimedia view)]. They should fold simultaneously to achieve twisting properties. Therefore, a parallelogram OAED is added to connect coplanar facet pairs OAB and OCD [Fig. 1(b)]. When all four facet pairs in the two eggboxes are connected in this way, an interconnected unit is obtained. The unit twists anticlockwise when compressed and twists clockwise when elongated, and so we define it as an RH chiral unit. If we change the connection segment to the parallelogram OBFC [Fig. 1(c)], an LH chiral unit is obtained, which twists clockwise when compressed.

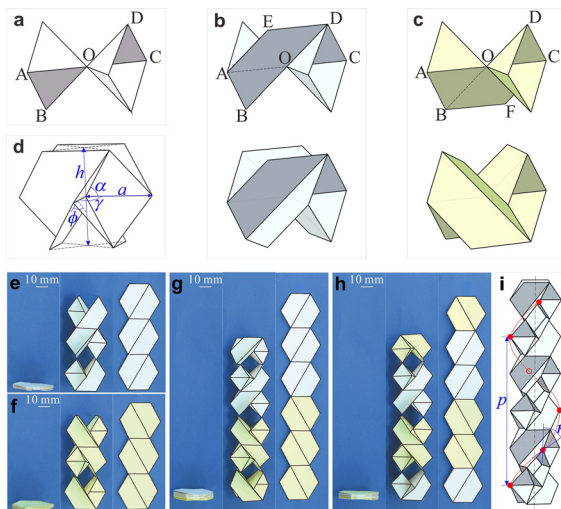


**FIG. 1.** Geometry of the origami-inspired chiral structure. (a) A basic element composed of two eggbox origami patterns. (b) and (c) Construction of a right-handed (RH, in gray-white) and a left-handed (LH, in yellow) unit, where the dotted line represents the crease behind. (d) Geometrical parameters in the chiral unit. (e)–(h) Paper model photographs of chiral and achiral structures, where the left, middle, and right figures represent the fully folded, partly elongated, and fully elongated configurations, respectively: (e) an RH chiral structure, (f) an LH chiral structure, (g) an achiral structure with the unit arrangement of RH-RH-RH-LH-LH-LH (top to bottom), and (h) an achiral structure with the unit arrangement of LH-RH-RH-LH-LH-LH. (i) Geometrical parameters in the chiral structure. Multimedia view: <https://doi.org/10.1063/5.0005336.1>

Two design parameters,  $a$  and  $\alpha$ , are adopted to characterize the chiral unit [Fig. 1(d)], which are the lateral edge length and sector angle of the eggbox, respectively. To quantitatively analyze the chirality, three more parameters are introduced, where  $\phi$  is the dihedral angle between the two lower trapezoid facets (i.e., the unit configuration angle),  $\gamma$  is the angle between the two horizontal alternative creases (i.e., the unit twist angle), and  $h$  is the distance between the bottom and top faces (i.e., the unit height). See detailed information in [supplementary material II](#).

By connecting identical chiral units at parallel edges on the bottom or top faces, we can obtain homogeneous RH or LH chiral structures. The rotational angle and distance between top and bottom faces of the structure are defined as the structural twist angle,  $\Gamma$ , and the structural height,  $H$ , respectively. Since we place chiral units in series, we have  $\Gamma = N\gamma$  and  $H = Nh$ , where  $N$  is the number of units in the structure. Figure 1(e) presents photographs of an RH chiral paper model constructed by three RH units with  $\alpha = 60^\circ$ . Similarly, we can obtain an LH chiral structure [Fig. 1(f)]. The chirality of the structure is characterized by a virtual helix formed by connecting the same vertex in each unit, as indicated by the red line in Fig. 1(i). The helical pitch and helical angle of the structure are  $p$  and  $\kappa$ , respectively (see [supplementary material II](#) for more information about the helix).

Additionally, heterogeneous chiral structures can be generated by mixing RH and LH units. The expressed chirality of the structure is determined by the number of RH and LH units, whereas the arrangement of these units changes only the internal twist angle in the structure. An achiral structure will be obtained when the numbers of RH and LH units are equal. For example, Fig. 1(g) shows an achiral structure with a maximum internal twist angle of  $360^\circ$ . If we change the arrangement of chiral units as shown in Fig. 1(h), the structure remains achiral, but with a decreased maximum internal twist angle of  $120^\circ$ .

Chirality of single chiral structures can be tuned by adjusting their design parameters, i.e., the sector angle,  $\alpha$ , the unit length,  $a$ , and the number of units,  $N$ . While  $a$  has no effect on chirality and the effect of  $N$  is linear, we focus on achieving chirality tunability by modulating  $\alpha$  here. We studied three cases of  $\alpha = 40^\circ$ ,  $60^\circ$ , and  $80^\circ$ . The relationship among the non-dimensional unit height,  $h/a$ , the unit twist angle,  $\gamma$ , and the unit configuration angle,  $\phi$ , is presented in Fig. 2(a) (Multimedia view). When we fold the chiral unit ( $\phi$  increases from  $0^\circ$  to  $180^\circ$ ),  $\gamma$  increases to  $2\alpha$  and  $h$  decreases to zero. We found that for a given  $\phi$ , a larger  $\alpha$  corresponds to larger  $h/a$  and  $\gamma$  values. Hence, a chiral structure with a larger  $\alpha$  is more twisted when equally folded.

The folding of chiral units generates helical winding of the whole structure. In general,  $\kappa$  is taken as the characteristic quantity for a helical structure. During the folding process, no matter the value of  $\alpha$ ,  $p$  reduces to zero, whereas  $\kappa$  increases to  $\pi/2$  due to  $\frac{p}{a} = \frac{2\pi}{\tan \kappa}$ . The relationship between  $\kappa$  and  $\phi$  is presented in Fig. 2(b). It shows that  $\kappa$  is positively related to  $\alpha$  when  $\phi$  is kept constant, meaning that a larger  $\alpha$  generates a more highly wound helix. With the increase in  $\kappa$ ,  $p/a$  and  $h$  decrease, whereas  $\gamma$  increases [Figs. 2(c) and 2(d)]. Furthermore, the helix winds along with the twisting of chiral units. The coupling between them is revealed by the relationship curve between  $\gamma$  and  $\kappa$  in Fig. 2(d), which shows that for helices with identical  $\kappa$ , a larger  $\alpha$  always produces a larger  $\gamma$ , i.e., requires fewer units to complete a full helix turn.

The phenomena described for RH chiral models with different  $\alpha$  values are demonstrated experimentally in Fig. 2(e), where three representative configuration photographs are shown for each paper model

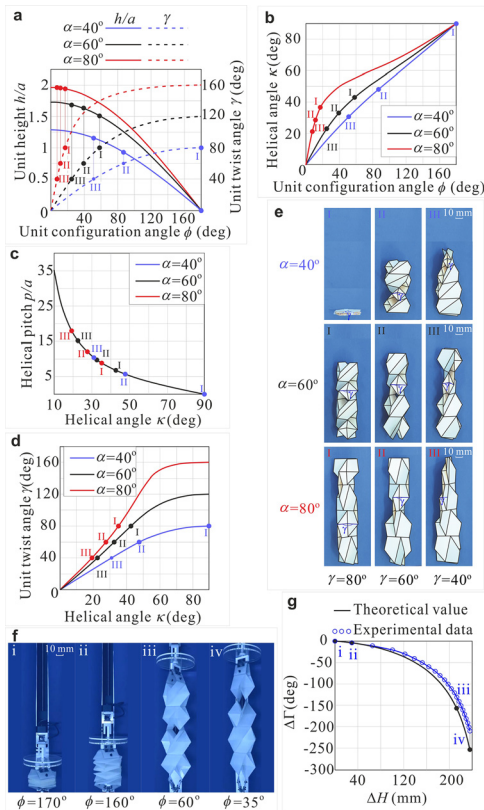


**FIG. 2.** Helical characteristics of the RH chiral structure when  $\alpha$  values are  $40^\circ$  (blue line),  $60^\circ$  (black line), and  $80^\circ$  (red line). (a) Relationship among  $h/a$ ,  $\gamma$ , and  $\phi$ . (b) Relationship between  $\kappa$  and  $\phi$ . (c) Relationship between  $p/a$  and  $\kappa$ . (d) Relationship between  $\gamma$  and  $\kappa$ . (e) Three configuration photographs of the paper models with different twist angles during twisting. Roman numerals I, II, and III in panels (a)–(e) represent configurations with  $\gamma = 40^\circ$ ,  $60^\circ$ , and  $80^\circ$ , respectively. (f) Tensile experiment of the RH structure with  $\alpha = 60^\circ$  and  $a = 40$  mm; four representative configuration photographs are presented during the experiment. (g) Theoretical (black line) and experimental (blue dots) twist angle increment,  $\Delta\Gamma$ , vs height increment,  $\Delta H$ . Roman numerals i, ii, iii, and iv correspond to different stages during tensile testing shown in panel (f). Multimedia view: <https://doi.org/10.1063/5.0005336.2>

with  $\gamma = 40^\circ$ ,  $60^\circ$ , and  $80^\circ$ . The structural height increased with a reduction in  $\gamma$  for all cases. However, the structure is less folded with a larger  $\alpha$ , leading to a larger height for a given  $\gamma$ . Therefore, we can tune  $\alpha$  to design chiral structures with desired properties of helices (e.g., height, degree of folding, etc).

The analytical results were validated through a tensile experiment on a homogeneous RH chiral structure with  $N = 4$  and  $\alpha = 60^\circ$  (see [supplementary material V](#) for details). Four representative configuration photographs of the structure during the tension process are presented in [Fig. 2\(f\)](#). The theoretical and experimental relationships between the structural twist angle increment,  $\Delta\Gamma$ , and the structural height increment,  $\Delta H$ , are presented as blue dots and black lines in [Fig. 2\(g\)](#), respectively, wherein  $a = 40$  mm,  $\Delta\Gamma = \Gamma - \Gamma_0$ ,  $\Delta H = H - H_0$ , and  $\Gamma_0$  is the initial structural twist angle when  $H_0 = 25$  mm. The experimental data match well with the analytical results, and  $\Delta\Gamma$  decreases exponentially as  $\Delta H$  increases. The slight deviation of the experimental data is mainly due to the small rotational

stiffness of creases in the physical specimen, whereas that in the theoretical model is assumed to be zero.

We have characterized twisting and helical properties of homogeneous RH structures and demonstrated chirality tunability. The same behavior would be expected for LH structures, as only the handedness changes in these structures, with helical properties remaining the same. Next, we extend our model to achieve chirality switching and hierarchy.

In general, the chirality of a designed structure is fixed. It is challenging to achieve chirality switching in man-made chiral structures owing to the different construction of RH or LH structures. This problem also exists in our paper models: the movement of the structure in [Fig. 3\(a\)](#) (Multimedia view) terminates when the model reaches the fully elongated state owing to facet interference. From a mechanistic perspective, the chiral structure can be regarded as a network of spherical 4R and planar 4R linkages,<sup>29</sup> and different chirality corresponds to different motion branches of the linkage network. So we can achieve chirality switching through mechanism bifurcation. We redesign the structure to avoid facet interference while maintaining its bifurcation property. Hence, in [Fig. 3\(a\)](#), paper facets are replaced with curved links without changing their rotational axes to keep the kinematic equivalency. Taking advantage of the bifurcation of spherical 4R and planar 4R linkages, an RH chiral structure is capable of transforming

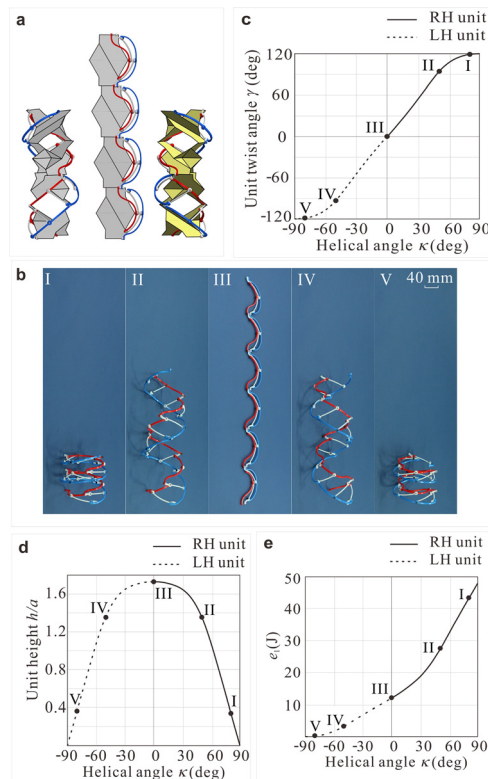


**FIG. 3.** RH and LH chirality switching. (a) Design of the switchable chiral structure: the link model can achieve the switching, whereas the paper model cannot. (b) Five configuration photographs of the 3D-printed and manually assembled linkage model during RH and LH chirality switching. (c) Relationship between  $\gamma$  and  $\kappa$  during chirality switching. (d) Relationship between  $h/a$  and  $\kappa$  during chirality switching. (e) Relationship between  $\epsilon_1$  and  $\kappa$  during chirality switching. Multimedia view: <https://doi.org/10.1063/5.0005336.3>

into an LH one through the fully elongated configuration or *vice versa*. This chirality switching process is presented in Fig. 3(b), where configurations I and II correspond to RH chirality, IV and V to LH chirality, and III to the critical singularity position where the switching occurs.

To determine the variation in twisting and helical properties during chirality switching, we plotted  $\gamma$  and  $h/a$  as functions of  $\kappa$  in Figs. 3(c) and 3(d), respectively. This analysis reveals that the switching occurs in the fully elongated configuration where  $\kappa = 0^\circ$  and  $\gamma = 0^\circ$ . This switching behavior is different from most previously reported examples, where chirality switching is induced by external stimuli,<sup>14–17,22</sup> and also from the spontaneous chirality switching found in bacterial flagella, which only occurs in partial regions.<sup>19</sup> Since the chirality switching in the structure is achieved by mechanism bifurcation, it can be fabricated and controlled more easily compared to existing ones with molecular structural changes. Because of the switching, the range of helical angles is expanded to  $[-90^\circ, 90^\circ]$ , which is twice that of the paper structure presented in Figs. 1 and 2. To figure out the required energy for chirality switching, we assume that there is no deformation in the links and the energy of the structure is mainly stored in the joints. We add a torsional spring in each joint, whose stiffness coefficient is defined as  $k_1$ . The energy of the whole structure is then the total elastic potential energy in all joints. We assume that the energy of a single chiral unit (defined as  $e_1$ ) is zero when the structure is in the fully folded LH configuration. The relationship between  $e_1$  and  $\kappa$  during chirality switching is then derived and plotted in Fig. 3(e), where  $k_1 = 0.4 \text{ N} \cdot \text{m}/\text{rad}$ . The required energy of chirality switching is the energy of the structure in the switch configuration where  $\phi = 0$  [configuration III in Fig. 3(b)], which is found to be  $17k_1\pi^2$ . Therefore, we can only lower the energy cost for chirality switching by reducing the stiffness coefficient  $k_1$ . The detailed calculation is given in [supplementary material II](#).

To achieve a hierarchically chiral structure with more helices, the apex of each eggbox should not be located along the same axis as in Figs. 1 and 2, which requires the change in the connection between adjacent chiral units. The chiral construction unit is altered to a more general unit [Fig. 4(a) (Multimedia view)], where one additional parameter,  $\beta$ , is introduced, which is the sector angle of the connection part. The creases of the connection part are presented as dashed lines in Fig. 4(b). The hierarchically chiral structure has two helices, which are defined as the major helix and the minor helix and presented as thick and thin red lines in Fig. 4(c), respectively. The major helix is formed by the apex of each eggbox, whereas the minor helix is formed by one identical vertex in the base of each eggbox, which is the same as the single helix in our paper model shown in Fig. 1(i). Similar to previously reported synthetic hierarchically chiral structures,<sup>23,24,28</sup> our structure transfers chirality at the same macroscale. Four parameters,  $K$ ,  $P$ ,  $R$ , and  $L$ , are introduced to characterize the major helix, which are the helical angle, helical pitch, radius, and length along the helical axis, respectively (see [supplementary material III](#) for detailed information about these helices).

We then analyzed helical properties of the hierarchically chiral structure. With the introduction of the major helix, an unusual property of the hierarchically chiral structure arises compared to the existing synthetic and biological ones with the monotonically increasing height during the unwinding process, namely, the height of the structure first increases from zero to the maximum value and then decreases to zero when being unwound, as shown in Fig. 4(d). Physical model photographs of five representative configurations

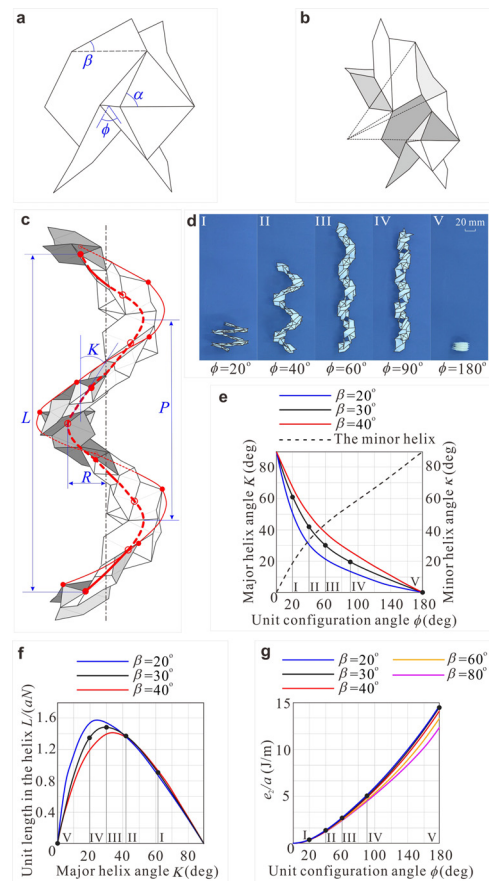


**FIG. 4.** Design and helical characteristics of the hierarchically chiral structure (a) Altered chiral construction unit for the structure. (b) Two altered units are connected. (c) Geometrical parameters in the structure, where the thick and thin red lines represent the major helix and the minor helix, respectively. (d) Five configuration photographs of the structure, where  $\phi$  values are 20°, 40°, 60°, 90°, and 180°. (e) Relationship between  $K$ ,  $\kappa$ , and  $\phi$ ; (f) Relationship between  $L/(aN)$  and  $K$ ; (g) Relationship between  $e_1/a$  and  $\phi$ . Multimedia view: <https://doi.org/10.1063/5.0005336.4>

made of 12 RH units with  $\alpha = 60^\circ$  and  $\beta = 30^\circ$  are presented. The major and minor helices have identical chirality, while those for the existing hierarchically chiral structures can be different, indicating that constituent units dominate the chirality of our structure. However, helical properties of the major and minor helices differ greatly. With the folding of the structure, the minor helix winds, while the major helix unwinds; that is,  $K$  decreases, whereas  $\kappa$  (the angle between the minor helix and its axial line—the major helix) increases, as indicated by the solid and dashed black lines in Fig. 4(e), respectively. Since the basic vertices forming the major helix and the minor helix are in the same chiral unit, their windings are coupled, while the existing hierarchically chiral structures have independent winding. In contrast to the single-helix case with a monotonically decreasing pitch and unit length during winding, the unit length,  $L/(aN)$ , of the major helix first increases and then decreases, as shown in Fig. 4(f). The energy of the hierarchically chiral structure can also be calculated by the torsional spring model. Supposing that the stiffness coefficient per unit length of the spring in each crease of the structure is  $k_2$  and assuming that the

unit elastic potential energy  $e_2 = 0$  when  $\phi = 0$ , we can then obtain the relationship between  $e_2/a$  and  $\phi$  with five different values of  $\beta$  when  $\alpha = 60^\circ$ , as illustrated in Fig. 4(g) (in which  $k_2 = 0.3 \text{ N/rad}$ ). This indicates that the energy of the structure can be tuned by  $\beta$ . Less energy is required for the movement of the structure if a larger  $\beta$  is selected (see supplementary material III for the detailed calculation).

In summary, we proposed helical units and structures based on eggbox-shaped origami and tuned their chirality by adjusting geometrical parameters. They can be used as theoretical models to understand the mechanism of chirality in nature. For example, our proposed achiral structure is similar to the helical towel gourd tendrils with opposite handedness when climbing with a hook to a supporting object. Studying the movement of our model helps to better understand the chiral growth mechanism of these tendrils. Switchable chirality was achieved through the bifurcation of kinematically equivalent linkages, which will make it possible to alter the on-sight optical or electromagnetic properties of the metamaterial constructed from such helical units. We also designed hierarchically chiral structures with major and minor helices at the same macroscale, while the winding of the minor helix drives the unwinding of the major helix. Such an unusual behavior, resulting in two compact folding configurations, provides an opportunity to design multi-functional morphing structures in aerospace engineering. Furthermore, due to its single degree of freedom, the chiral structures proposed here will be applied to the bionic robots with a simple control system in our next step research.

Origami has been presented as an effective way to design reconfigurable structures and metamaterials<sup>30–37</sup> and exhibited great potential in those with chiral or hierarchical properties. Besides the eggbox, there are many other typical patterns, some of which demonstrate chiral behavior during folding, while tessellation plays an important role in constructing hierarchical structures. Normally, the rigid pattern is preferred to get reliable deformation and the non-rigid one provides the bi-stable property. We can foresee that the present approach can be applicable to origami units for different widely designed targets, not limited to the chirality.

See the supplementary material for detailed derivations, equations, figures, and tables.

## AUTHORS' CONTRIBUTIONS

H.F. and W.L. contributed equally to this work. H.F., J.M., and Y.C. wrote this manuscript. H.F. and Y.C. proposed the construction method of the chiral units and helical structures inspired from the miracle hexagon designed by W. C. W.L. conducted the experiment and designed the structure with switchable and hierarchical chirality under the supervision of J.M. and Y.C. H.F., and W.L. prepared all the figures and supplementary material. J.W. provided advice on the analysis of chiral structures.

Y.C. acknowledges the support of the National Natural Science Foundation of China (Project Nos. 51825503 and 51721003); J.M. acknowledges the support of the National Natural Science Foundation of China (Project No. 51575377).

The authors declare no competing financial interest.

## REFERENCES

- W. J. Lough and I. W. Wainer, *Blackwell Science* (Oxford, 2002).
- W. Wu, W. Hu, G. Qian, H. Liao, X. Xu, and F. Berto, *Mater. Des.* **180**, 107950 (2019).
- P. X. Gao, Y. Ding, W. Mai, W. L. Hughes, C. Lao, and Z. L. Wang, *Science* **309**(5741), 1700 (2005).
- J. S. Wang, X. Q. Feng, J. Xu, Q. H. Qin, and S. W. Yu, *J. Comput. Theor. Nanoscience* **8**(7), 1278 (2011).
- B. Pendry, *Science* **306**(5700), 1353 (2004).
- C. Huang, Y. Feng, J. Zhao, Z. Wang, and T. Jiang, *Phys. Rev. B* **85**(19), 195131 (2012).
- S. Heeg, L. Shi, L. V. Poulikakos, T. Pichler, and L. Novotny, *Nano Lett.* **18**(9), 5426 (2018).
- D. M. Tang, D. G. Kvashnin, O. Cretu, Y. Nemoto, F. Uesugi, M. Takeguchi, X. Zhou, F. C. Hsia, C. Liu, P. B. Sorokin, N. Kawamoto, M. Mitome, H. M. Cheng, D. Goldberg, and Y. Bando, *Ultramicroscopy* **194**, 108 (2018).
- Z. Wang, L. Jing, K. Yao, Y. Yang, B. Zheng, C. M. Soukoulis, H. Chen, and Y. Liu, *Adv. Mater.* **29**(27), 1700412 (2017).
- H. Yasuda, T. Tachi, M. Lee, and J. Yang, *Nat. Commun.* **8**(1), 962 (2017).
- M. D. Turner, M. Saba, Q. Zhang, B. P. Cumming, G. E. Schröder-Turk, and M. Gu, *Nat. Photonics* **7**(10), 801 (2013).
- Y. Yang, R. C. Da Costa, M. J. Fuchter, and A. J. Campbell, *Nat. Photonics* **7**(8), 634 (2013).
- S. Stampfer, A. Jungen, R. Linderman, D. Obergefell, S. Roth, and C. Hierold, *Nano Lett.* **6**(7), 1449 (2006).
- X. Lan, T. Liu, Z. Wang, A. O. Govorov, H. Yan, and Y. Liu, *J. Am. Chem. Soc.* **140**(37), 11763 (2018).
- K. Murata, M. Aoki, T. Suzuki, T. Harada, H. Kawabata, T. Komori, F. Ohseto, K. Ueda, and S. Shinkai, *J. Am. Chem. Soc.* **116**(15), 6664 (1994).
- J. de Jong, L. N. Lucas, R. M. Kellogg, J. H. van Esch, and B. L. Feringa, *Science* **304**(5668), 278 (2004).
- M. Suda, Y. Thathong, V. Promarak, H. Kojima, M. Nakamura, T. Shiraogawa, M. Ehara, and H. M. Yamamoto, *Nat. Commun.* **10**(1), 2455 (2019).
- D. Coombs, G. Huber, J. O. Kessler, and R. E. Goldstein, *Phys. Rev. Lett.* **89**(11), 118102 (2002).
- M. Schäferling, D. Dregely, M. Hentschel, and H. Giessen, *Phys. Rev. X* **2**(3), 031010 (2012).
- E. Plum, V. A. Fedotov, and N. I. Zheludev, *J. Opt. A* **11**(7), 074009 (2009).
- L. Wu, Z. Yang, Y. Cheng, Z. Lu, P. Zhang, M. Zhao, R. Gong, X. Yuan, Y. Zheng, and J. Duan, *Opt. Express* **21**(5), 5239 (2013).
- S. Zhang, J. Zhou, Y. S. Park, J. Rho, R. Singh, S. Nam, A. K. Azad, H. Chen, X. Yin, A. J. Taylor, and X. Zhang, *Nat. Commun.* **3**, 942 (2012).
- Z. L. Zhao, H. P. Zhao, J. S. Wang, Z. Zhang, and X. Q. Feng, *J. Mech. Phys. Solids* **71**, 64 (2014).
- B. Pokroy, S. H. Kang, L. Mahadevan, and J. Aizenberg, *Science* **323**(5911), 237 (2009).
- J. S. Wang, G. Wang, X. Q. Feng, T. Kitamura, Y. L. Kang, S. W. Yu, and Q. H. Qin, *Sci. Rep.* **3**, 3102 (2013).
- J. S. Wang, Y. H. Cui, T. Shimada, H. P. Wu, and T. Kitamura, *Appl. Phys. Lett.* **105**(4), 043702 (2014).
- Y. Yang, J. Liang, F. Pan, Z. Wang, J. Zhang, K. Amin, J. Fang, W. Zou, Y. Chen, X. Shi, and Z. Wei, *Nat. Commun.* **9**(1), 3808 (2018).
- J. L. Jimenez, E. J. Nettleton, M. Bouchard, C. V. Robinson, C. M. Dobson, and H. R. Saibil, *Proc. Natl. Acad. Sci. U. S. A.* **99**(14), 9196 (2002).
- S. Dai and J. R. Jones, *J. Mech. Des.* **121**(3), 375 (1999).
- B. Liu, J. L. Silverberg, A. A. Evans, C. D. Santangelo, R. J. Lang, T. C. Hull, and I. Cohen, *Nat. Phys.* **14**(8), 811–815 (2018).
- J. L. Silverberg, A. A. Evans, L. McLeod, R. C. Hayward, T. Hull, C. D. Santangelo, and I. Cohen, *Science* **345**(6197), 647–650 (2014).
- J. T. Overvelde, T. A. De Jong, Y. Shevchenko, S. A. Becerra, G. M. Whitesides, J. C. Weaver, C. Hoberman, and K. Bertoldi, *Nat. Commun.* **7**(1), 10929 (2016).
- K. Bertoldi, V. Vitelli, J. Christensen, and M. van Hecke, *Nat. Rev. Mater.* **2**(11), 17066 (2017).
- S. Waitukaitis, R. Menaut, B. G. G. Chen, and M. van Hecke, *Phys. Rev. Lett.* **114**(5), 055503 (2015).
- Y. Tang, G. Lin, S. Yang, Y. K. Yi, R. D. Kamien, and J. Yin, *Adv. Mater.* **29**(10), 1604262 (2017).
- M. B. Pinson, M. Stern, A. C. Ferrero, T. A. Witten, E. Chen, and A. Murugan, *Nat. Commun.* **8**(1), 15477 (2017).
- M. Stern, M. B. Pinson, and A. Murugan, *Phys. Rev. X* **7**(4), 041070 (2017).